NANO LETTERS

Letter

Enabling Ultrahigh Plastic Flow and Work Hardening in Twinned Gold Nanowires

Chuang Deng, and Frederic Sansoz

Nano Lett., **2009**, 9 (4), 1517-1522• DOI: 10.1021/nl803553b • Publication Date (Web): 16 March 2009

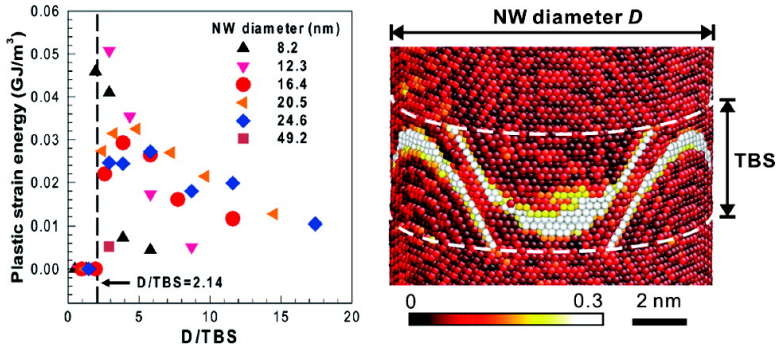

More About This Article

Additional resources and features associated with this article are available within the HTML version:

- Supporting Information
- Access to high resolution figures
- Links to articles and content related to this article
- Copyright permission to reproduce figures and/or text from this article

View the Full Text HTML

NANO LETTERS

2009
Vol. 9, No. 4
1517-1522

Enabling Ultrahigh Plastic Flow and Work Hardening in Twinned Gold Nanowires

Chuang Deng and Frederic Sansoz*

School of Engineering and Materials Science Program, The University of Vermont, Burlington, Vermont 05405

Received November 24, 2008; Revised Manuscript Received February 3, 2009

ABSTRACT

By using molecular dynamics simulations, we show that significant strain hardening and ultrahigh flow stresses are enabled in gold nanowires containing coherent (111) growth twins when balancing nanowire diameter and twin boundary spacing at the nanoscale. A fundamental transition in mechanical behavior occurs when the ratio of diameter to twin boundary spacing is larger than 2.14. A model based on site-specific dislocation nucleation and cross-slip mechanisms is proposed to explain the size dependence of flow behavior in twinned nanowires under tensile loading.

The bulk strength of pure metals such as gold is governed by the ability of crystals to harden upon plastic strain, or strain hardening.[1] Past experimental and atomistic simulation studies[2−7] have revealed that unlike bulk metals, gold nanowires (NWs) with diameters up to 50 nm[8−11] generally exhibit ultrahigh strength followed by a sharp yield point and severe strain softening when deformed under tensile or compressive loading, similar to the behavior of defect-free gold whiskers.[12] Achieving control over strain hardening effects in gold NWs is critically important to ultimately boost their role as structural building blocks in nanotechnology.

A classical picture of strain hardening in pure-metal single crystals has been derived for some time from the processes of emission, glide, and interactions of dislocations, or linear defects.[1] A stage in which dislocations can move easily without encountering barriers leads to little hardening (Stage I), while Stage II hardening corresponds to a rapid increase in the applied stress required to produce plastic strain as the density of preexisting dislocations or obstacles increases. Most microplasticity experiments and simulations in pure face-centered cubic (fcc) metals have recently shown clear evidence that Stage II hardening ceases to be valid when the specimen size falls in the submicron range, even for a high initial dislocation density, as dislocations can freely escape at free surfaces by making the crystal small enough.[2,13−16]

Therefore, in order to increase work hardening and flow stresses in metal NWs, special defects must be added to prevent the easy glide of dislocations and their exhaustion at free surfaces without compromising the sample strength. A new concept, which consists in introducing high densities of coherent nanoscale twins, has recently emerged and was found very successful in increasing both strength and ductility in some bulk polycrystalline metals with low-stacking fault energy.[17−20] Coherent twin boundaries (CTBs) are low-energy, planar defects widely observed in metallic thin films[18] and are even more common in metal NWs.[8,9,11,21,22] The mechanistic interactions between lattice dislocations and CTBs have been analyzed in detail by molecular dynamics (MD) simulations.[5,7,23−29] However, a predictive understanding of the effects of specimen size on hardening mechanisms in twinned NWs has proved elusive. Although CTBs were found to be strong obstacles to the glide of dislocations,[7,23−29] only limited increase in strain hardening has been reported so far in twinned NWs. Here, using large-scale MD simulations, we report that significant strain hardening and ultrahigh flow stresses are enabled in twinned gold NWs when the NW diameter increases or, conversely, the twin boundary spacing decreases at the nanoscale.

In this study, MD simulations were performed using LAMMPS[30] with an embedded-atom-method (EAM) potential for gold developed by Grochola et al.[31] This potential gives realistic values for the stacking fault energy of gold ($\gamma_{SF}^{EAM} = 43.4$ mJ•m^{-2}) as compared to experimental data ($\gamma_{SF}^{Exp} = 32\sim46.4$ mJ•m^{-2}).[31] NWs were created with a cylindrical shape and oriented along the [111] direction. A periodic boundary condition was imposed along the NW axis, while the NW was kept free in the other directions. The models varied from 100 000 to 15 million atoms depending on the NW size. The simulations were carried out using a Verlet

* To whom correspondence should be addressed. Phone: 802 656 3837. Fax: 802 656 1929. E-mail: frederic.sansoz@uvm.edu.

10.1021/nl803553b CCC: $40.75
Published on Web 03/16/2009

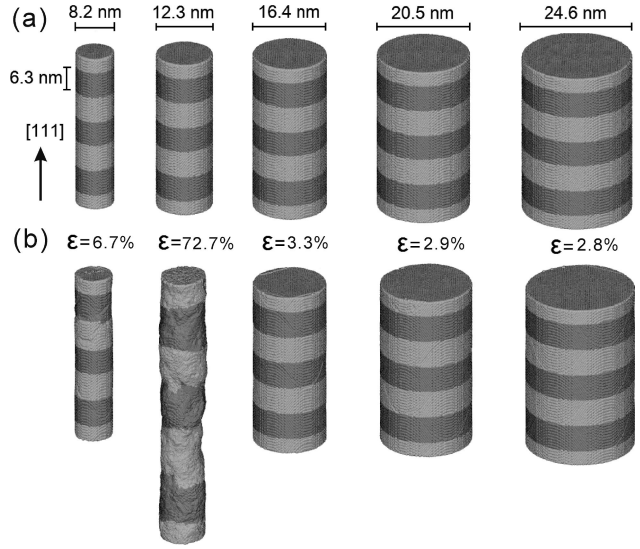

Figure 1. Effect of specimen diameter on nanoscale plasticity in [111]-oriented, cylindrical gold nanowires with 6.3 nm twinned superlattice. (a) Relaxed structures before loading. (b) Same structures after 100 ps under constant tensile stress of 3.2 GPa. The nanowire with a diameter of 12.3 nm clearly exhibits the lowest resistance and most significant elongation (ε).

algorithm with a time step of 5 fs. Each model was relaxed before deformation for 20 000 steps (100 ps) under zero stress. The simulations shown in Figure 1 were performed by applying a constant tensile stress of 3.2 GPa along the [111] direction and zero stress in the other directions using constant NPT integration. In all other simulations, the NW was deformed at a constant strain rate of 2.7×10^7 s^{-1} along the [111] axis using constant NVT integration. All the simulations were performed at 300 K. The tensile stress was calculated by adding the local atomic stress along the loading direction calculated from the Virial theorem over all atoms in the cylinder and dividing by the deformed cylinder volume.[32]

We first conducted a series of MD simulations to characterize the effect of diameter in [111]-oriented, cylindrical gold NWs containing parallel CTBs deformed under constant tensile stress. We used the same reference lengths (37.8 nm) and twin boundary spacing (TBS) (6.3 nm) for the NWs in this series but different diameters from 8.2 to 24.6 nm (Figure 1a). The same structures deformed after 100 ps at a constant stress of 3.2 GPa are presented in Figure 1b. This figure shows that, unlike the tensile behavior of defect-free single-crystal NWs where smaller is generally better,[2−6] the two smallest NWs in this group (with diameter of 8.4 and 12.3 nm) showed less resistance and more significant plastic elongation than the other NWs.

An essential aspect is that the strength of the weakest NW with a diameter of 12.3 nm in Figure 1b can be dramatically improved again by decreasing the TBS, as shown in Figure 2a on the simulated stress−strain curves obtained by imposing constant strain rate ($2.7 \times 10^7 s^{-1}$). This figure shows a pronounced shift in mechanical behavior from whiskerlike deformation to strain-hardened regime as the TBS decreases, while the elastic modulus obtained from the linear regime does not change (130 GPa). It is worth noting that the NW

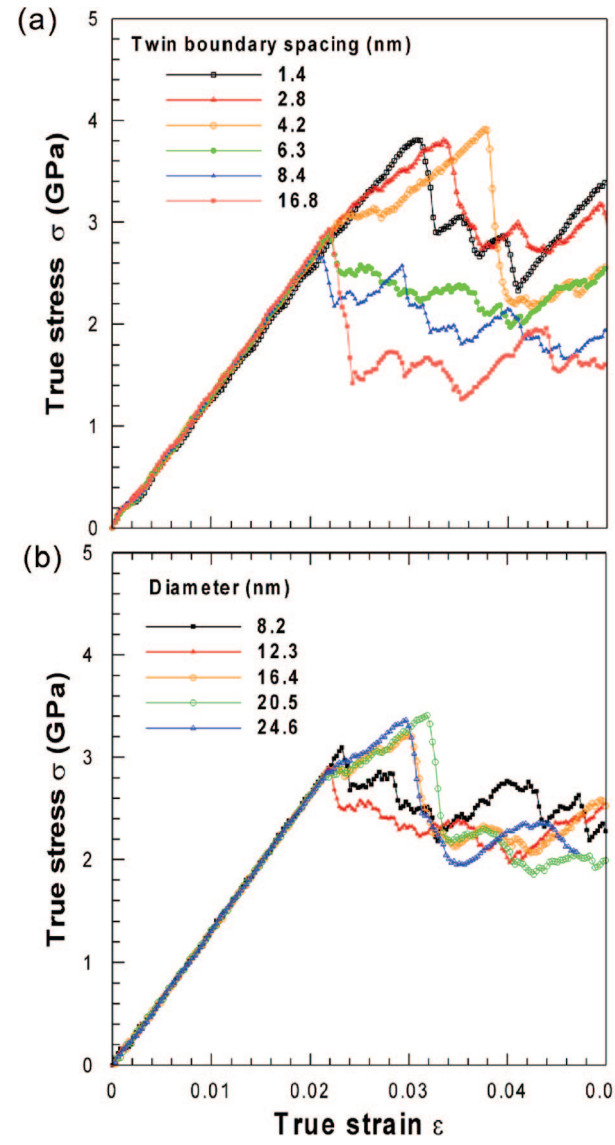

Figure 2. Size effects on the mechanical behavior of twinned gold nanowires under tensile loading at constant strain rate (2.7×10^7 s^{-1}). (a) Effect of twin boundary spacing on the $\sigma-\varepsilon$ curve of a 12.3 nm diameter twinned gold nanowire. (b) Effect of nanowire diameter on the $\sigma-\varepsilon$ curve of gold nanowires with same twin boundary spacing (6.3 nm). A transition in mechanical behavior from strain-softening (solid symbols) to strain-hardening (open symbols) is shown as the twin boundary spacing decreases or nanowire diameter increases.

with TBS equal to 6.3 nm has a maximum flow stress of 2.89 GPa followed by an abrupt drop in stress, which explains the low resistance of this NW at 3.2 GPa in Figure 1b. In contrast, the flow stress of the NW with TBS equal to 4.2 nm has been increased by 31% from 2.99 GPa at the elastic limit (2.3% strain) to 3.91 GPa at the maximum flow stress (3.8% strain). A similar trend was observed with an increase in NW diameter (Figure 2b).

The key to enabling maximum work hardening in gold NWs is therefore to find an optimum combination of NW diameter (D) and TBS. To this end, we introduced the concept of "normalized diameter" defined by the ratio of NW diameter to TBS, and performed MD simulations at constant strain rate with NW diameter ranging from 8.2 nm (100 000

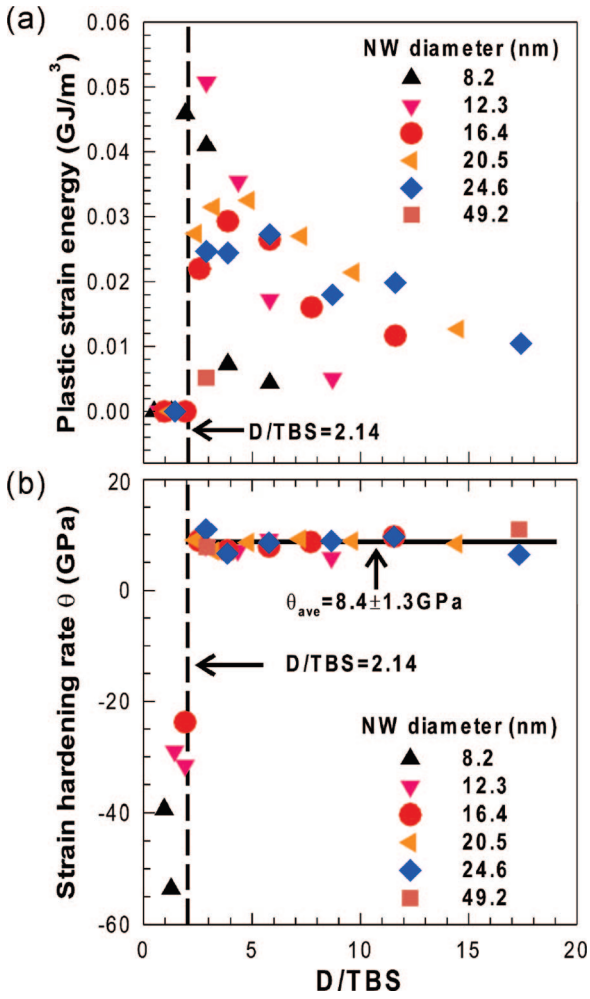

Figure 3. Effects of the normalized diameter (*D*/TBS) on plastic flow in twinned gold nanowires under tensile loading. (a) Plastic strain energy stored per unit volume. (b) Strain hardening rate θ. A cutoff dividing whiskerlike softening and Stage II strain hardening regimes is shown by a vertical dashed line for a normalized diameter of 2.14.

atoms) to 49.2 nm (15 million atoms) and TBS varying from 1.4 to 16.8 nm. The periodic length of each cylinder was fixed at 33.6 nm for all simulated NWs with $D < 49.2$ nm, and at 135.7 nm for the largest NWs with $D = 49.2$ nm. The plastic strain energy stored per unit volume and the strain hardening rate θ were determined for each NW (Supporting Information) and represented as a function of the normalized diameter in Figure 3a,b, respectively. These two figures show a clear discontinuity at a normalized diameter near 2, which divides the mechanical behavior of twinned NWs into two regimes. Above the cutoff, the NWs behave in a ductile manner with flow stresses significantly higher than yield stresses due to enhanced strain hardening while, below the cutoff, the NW behavior is quasi-brittle with negative strain hardening rate, that is, softening. It is also important to note that the strain hardening rate of all the NWs investigated above the cutoff is almost constant (8.4 ± 1.3 GPa) (Figure 3b), which strongly suggests that the mechanism of strain hardening is identical between these NWs. In addition, the plastic strain energy stored per unit volume of NWs above the cutoff is optimum when the normalized diameter approaches the cutoff value (Figure 3a).

In the present study, the yield of all NWs was found to occur by the emission of $1/6\{11\bar{1}\}\langle 112\rangle$ Shockley dislocations from the lines defining the intersection of CTBs with the free surface (Figure 4a and Supporting Information, Figure S2), which suggests the existence of specific sites for the nucleation of surface dislocations in twinned NWs. Furthermore, we present in Figure 4b a snapshot of deformation at maximum flow stress in a strain-hardened gold NW (D/TBS = 2.93). This figure shows only three favorable nucleation sites of identical source length per CTB at the free surface (see also Supporting Information, Figure S2). Using the atomic von Mises strain,[34] Figure 4c confirms the idea that the dislocation emission is predominantly site-specific and takes place at the intersection of the CTBs with the free surface. The CTBs were found to be strong barriers for the propagation of all leading partial dislocations emitted from the free surface until the maximum flow stress was reached, regardless of the NW diameter and TBS (for example, see Figure 4b and Supporting Information, Movies S1 and S2).

This analysis enables us to conclude that the existence of a transition from softening to strain hardening, as a function of normalized diameter, is mostly related to a difference in cross-slip mechanisms when slip is blocked by CTBs. The different slip pathways observed in Figure 4d,e for NWs with D/TBS equal to 1.95 and 2.93, respectively, corroborate this assumption. For NWs presenting no work hardening, the obstruction of the leading dislocations by CTBs rapidly evolves (<15 ps) to the transmission of the screw component of the dislocations onto adjacent $\{11\bar{1}\}$ planes, as shown in Figure 4d. Since for [111]-oriented NWs under tensile loading, the Schmid factor of the leading dislocations (0.314) is twice that of the trailing partial dislocation (0.157),[3] no trailing dislocations are emitted under this condition. However, the ability of the leading dislocations to freely transmit on adjacent slip planes stops, as shown in Figure 4e, when the normalized diameter becomes larger than 2.14 based on simple geometrical considerations (see Supporting Information). This limit agrees perfectly with the cutoff value found from simulations in Figure 3a,b. For D/TBS > 2.14, the only possibility of cross-slip mechanism is through the CTBs, as shown below, which occurs when the driving force is high enough to activate the slip of the trailing dislocations, thereby resulting in strong strain hardening effects.

The interactions between dislocations and CTBs have been explored in various fcc metals.[26−29] Zhu et al.[28] have modeled the slip transfer reactions of $1/2 < 1\bar{1}0>$ screw dislocations in copper at a CTB and predicted a pathway that involves the absorption of the incoming screw dislocation from the parent grain into the CTB, followed by desorption into the twin grain. In this pathway, the screw dislocation first dissociates into two Shockley partials (leading and trailing partial dislocation). However, the two partial dislocations have to constrict to a full screw dislocation at the CTB for the absorption and desorption mechanisms to proceed. Jin et al.[26,29] have found that in copper and nickel both screw

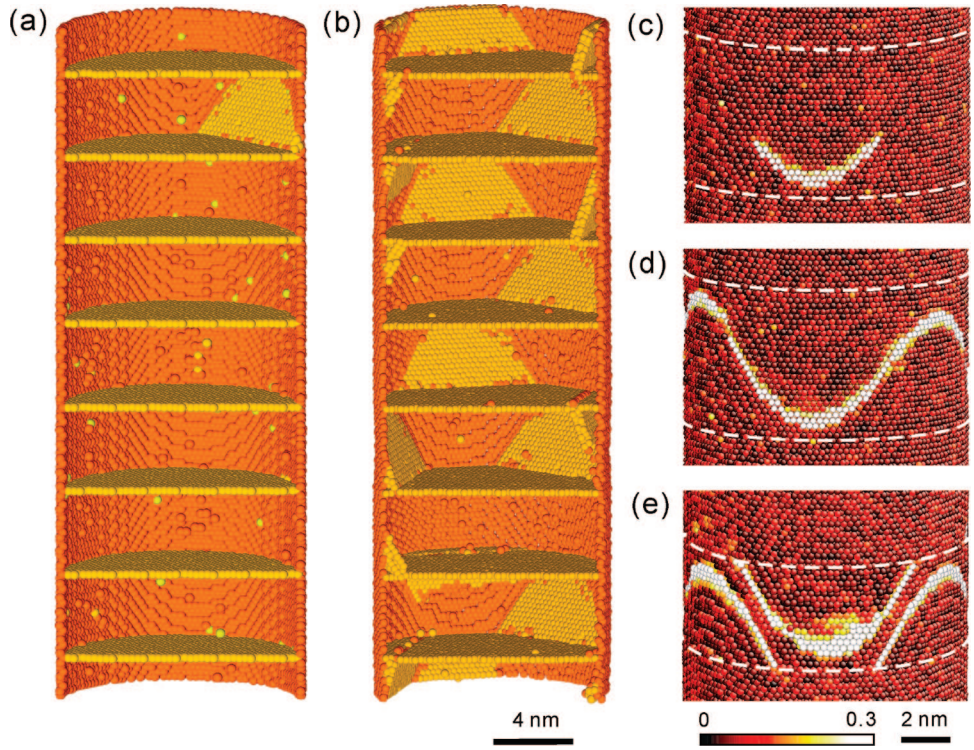

Figure 4. Dislocation nucleation and cross-slip mechanisms in twinned gold nanowires under tensile loading. (a) Snapshot of emission of the first dislocation and (b) deformation at maximum flow stress in a nanowire with $D = 12.3$ nm and TBS $= 4.2$ nm (D/TBS $=$ 2.93). Atom colors correspond to the local crystal structure.[32] Perfect fcc atoms and some atoms on the free surface and twin boundaries have been omitted for clarity. (c) Close-up view on the surface of a nanowire with $D = 12.3$ nm and TBS $= 6.3$ nm (D/TBS $= 1.95$) at the initial yielding and (d) 15 ps after yielding. (e) Close-up view on the surface of a nanowire with $D = 12.3$ nm and TBS $= 4.2$ nm (D/TBS $= 2.93$) at maximum flow stress, i.e., more than 560 ps after yielding. Atoms in panels c−e are colored using the atomic von Mises strain.[34]

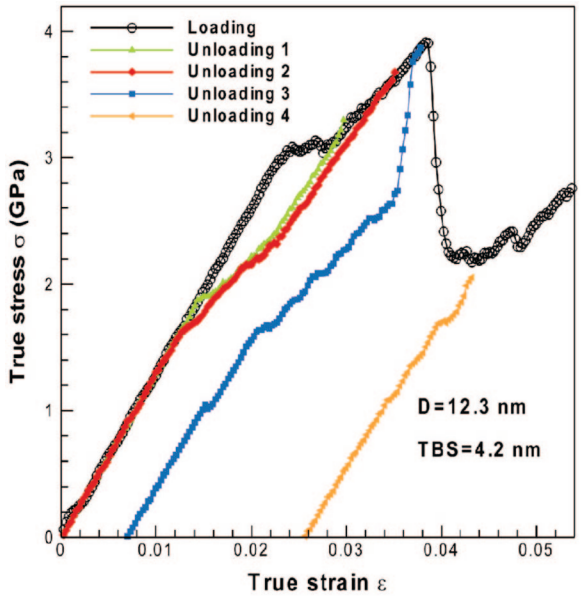

Figure 5. Simulated $\sigma-\varepsilon$ curve of a strain-hardened gold nanowire with 12.3 nm diameter and 4.2 nm twin boundary spacing during tensile loading and unloading. Plastic recovery is evident upon unloading at stages 1−3 of the strain hardening regime. No recovery is found after unloading at stage 4.

and nonscrew full dislocations dissociate into the leading and trailing Shockley dislocations at the beginning, and the dissociated leading partial dislocation cannot pass through the CTB before the trailing catches up to form a full dislocation. In another simulation study,[27] the CTB was also found to serve as a strong barrier to the leading partial dislocation. Thus if one can eliminate or delay the emission of the trailing partials, one can expect the leading partial dislocations to be stopped by the CTBs and produce hardening as observed in our simulations. Figure 5 shows that in strain-hardened gold NWs the leading partials do not immediately react with the CTBs, because plastic recovery occurs upon unloading at stages 1−3 of the strain hardening regime, as opposed to unloading at stage 4 after the pop-in event (see also Supporting Information, Movie S3). However, as soon as the trailing dislocations are emitted and reach the leading dislocations, full dislocations form and pass through the CTBs. Such a reaction causes an abrupt relief in flow stress, that is, somewhat leading to the failure of the NW.

Figure 6 and Supporting Information, Movie S4 show a detailed analysis of the slip mechanisms at the intersection between slip and several twin boundaries in a strain-hardened gold NW at peak stress with $D = 12.3$ nm and TBS $= 4.2$ nm (D/TBS $= 2.93$). Before cross-slip, a full dislocation was formed at CTB2 in the parent grain via the reaction

$$\frac{1}{6}(11\bar{1})[1\bar{2}\,\bar{1}] + \frac{1}{6}(11\bar{1})[\bar{1}\,\bar{1}\,\bar{2}] = \frac{1}{2}(11\bar{1})[0\bar{1}\,\bar{1}]$$

or, using Thompson's notations, $\quad B\gamma + \gamma D = BD \qquad (1)$

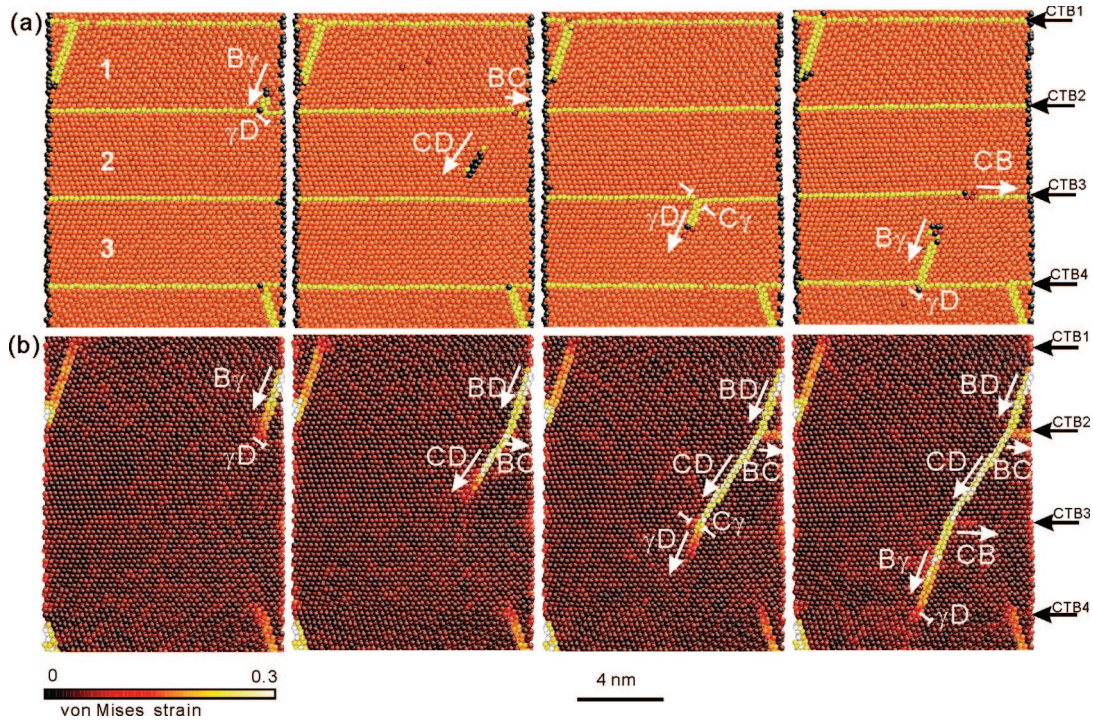

Figure 6. Cross-slip pathway at the intersection of slip with coherent twin boundaries in a gold nanowire with $D = 12.3$ nm and TBS = 4.2 nm after reaching the maximum flow stress. Atoms are colored by (a) Ackland and Jones' number[33] and (b) local von Mises strain.[34] The sequential dislocation reactions are (1) $B\gamma + \gamma D = BD$, (2) $BD = BC + CD$ at CTB2, and (3) $CD = C\gamma + \gamma D$, (4) $C\gamma = CB + B\gamma$ at CTB3. *BC* and *CB* are full dislocations gliding on the twin planes of CTB2 and CTB3, respectively, and moving toward the free surface. $B\gamma$ and γD are partial dislocations and $C\gamma$ is a sessile stair-rod dislocation on twin plane CTB3.

In eq 1, $1/6(11\bar{1})[\bar{1}\bar{1}\bar{2}]$ (γD) and $1/6(11\bar{1})[1\bar{2}\bar{1}]$ ($B\gamma$) are the leading and trailing partial dislocations, respectively. The full dislocation $1/2(11\bar{1})[0\bar{1}\bar{1}]$ (*BD*) is then transmitted to twin grain 2 by the reaction

$$\frac{1}{2}(11\bar{1})[0\bar{1}\,\bar{1}] = \frac{1}{2}(111)[10\bar{1}] + \frac{1}{2}(001)[\bar{1}\,\bar{1}0] \quad \text{or}$$
$$BD = BC + CD \qquad (2)$$

In eq 2, $1/2(001)[\bar{1}\bar{1}0]$ (*CD*) is the full dislocation transmitted in grain 2, and $1/2(111)[10\bar{1}]$ (*BC*) is a full dislocation gliding on the twin plane. Dislocation *CD* further reacts with CTB3 and is transmitted to twin grain 3 via the following reaction

$$\frac{1}{2}(001)[\bar{1}\,\bar{1}0] = \frac{1}{3}(112)[\bar{1}\,\bar{1}1] + \frac{1}{6}(11\bar{1})[\bar{1}\,\bar{1}\,\bar{2}] \quad \text{or}$$
$$CD = C\gamma + \gamma D \qquad (3)$$

In eq 3, $1/3(112)[\bar{1}\bar{1}1]$ ($C\gamma$) represents a sessile stair-rod dislocation at CTB3 that will further dissociate such as (see also Supporting Information, Figure S3):

$$\frac{1}{3}(112)[\bar{1}\,\bar{1}1] = \frac{1}{2}(111)[\bar{1}01] + \frac{1}{6}(11\bar{1})[1\bar{2}\,\bar{1}] \quad \text{or}$$
$$C\gamma = CB + B\gamma \qquad (4)$$

It is worth noting that the strain-hardening phenomenon observed in the present study on perfectly cylindrical gold NWs is largely related to the fact that the stress for nucleation of new dislocations on the wire surface is significantly smaller than that for the dislocation transmission at CTBs. Such a behavior could therefore be expected experimentally in NWs grown by electrodeposition in templates containing small cylindrical pores.[8,9] However, strain-hardening effects should also be expected in other types of twinned NWs with different surface structure and/or faceting, because it is known that surface faceting may lower the stress for dislocation nucleation without affecting the stress at which dislocations are blocked by the CTBs. For example, dislocations in twinned Cu NWs of square cross section have been predicted to nucleate at a lower stress than their circular counterparts.[35]

In summary, we have used atomistic simulations to reveal the existence of a fundamental limit dividing the mechanical behavior of twinned gold NWs into either strain softening or strain hardening regimes, as a function of the nanowire diameter and the number of twins (per unit length). Our theoretical study, which sheds light on a new approach to enable both ultrahigh tensile strength and improved ductility in nanoscale systems, will also stimulate further experimental progress to understand size effects in nanoscale crystal plasticity.

Acknowledgment. Support from NSF CAREER program (Grant DMR-0747658) and the computational resources provided by the Vermont Advanced Computing Center (NASA Grant NNX06AC88G) are gratefully acknowledged.

Supporting Information Available: (1) Mathematical derivations; (2) supporting figures; (3) online movies. This

material is available free of charge via the Internet at http://pubs.acs.org.

References

(1) Seeger, A. In *Dislocations and Mechanical Properties of Crystals*; Fisher, J. C., Johnston, W. G., Thomson, R., Eds.; John Wiley And Sons Inc.: New York, 1957, pp 243−329.
(2) Dow, R.; Derby, B. *Scr. Mater.* **2008**, *59*, 151.
(3) Diao, J.; Gall, K.; Dunn, M. L. *Nano Lett.* **2004**, *4*, 1863.
(4) Park, H. S.; Zimmerman, J. A. *Phys. Rev. B* **2005**, *72*, 054106.
(5) Hyde, B.; Espinosa, H. D.; Farkas, D. *JOM* **2005**, *57*, 62.
(6) Diao, J.; Gall, K.; Dunn, M. L.; Zimmerman, J. A. *Acta Mater.* **2006**, *54*, 643.
(7) Afanasyev, K. A.; Sansoz, F. *Nano Lett.* **2007**, *7*, 2056.
(8) Tian, M.; Wang, J.; Kurtz, J.; Mallouk, T. E.; Chan, M. H. W. *Nano Lett.* **2003**, *3*, 919.
(9) Wang, J.; Tian, M.; Mallouk, T. E.; Chan, M. H. W. *J. Phys. Chem. B* **2004**, *108*, 841.
(10) Wang, C.; Hu, Y.; Lieber, C. M.; Sun, S. *J. Am. Chem. Soc.* **2008**, *130*, 8902.
(11) Wu, B.; Heidelberg, A.; Boland, J. J. *Nat. Mater.* **2005**, *4*, 525.
(12) Brenner, S. S. Strength of gold whiskers. *J. Appl. Phys.* **1959**, *30*, 266.
(13) Greer, J. R.; Nix, W. D. *Phys. Rev. B* **2006**, *73*, 245410.
(14) Volkert, C. A.; Lilleodden, E. T. *Philos. Mag.* **2006**, *86*, 5567.
(15) Shan, Z. W.; Mishra, R. K.; Syed Asif, S. A.; Warren, O. L.; Minor, A. M. *Nat. Mater.* **2007**, *7*, 115.
(16) Benzerga, A. A. *Int. J. Plast.* **2008**, *24*, 1128.
(17) Lu, L.; Shen, Y.; Chen, X.; Qian, L.; Lu, K. *Science* **2004**, *304*, 422.
(18) Zhang, X.; et al. *Appl. Phys. Lett.* **2004**, *84*, 1096.
(19) Ma, E.; et al. *Appl. Phys. Lett.* **2004**, *85*, 4932.
(20) Dao, M.; Lu, L.; Shen, Y. F.; Suresh, S. *Acta. Mater.* **2006**, *54*, 5421.
(21) Sansoz, F.; Huang, H.; Warner, D. H. *JOM* **2008**, *60*, 79.
(22) Wu, B.; Heidelberg, A.; Boland, J. J. *Nano Lett.* **2006**, *6*, 468.
(23) Wang, J.; Huang, H. *Appl. Phys. Lett.* **2006**, *88*, 203112.
(24) Cao, A. J.; Wei, Y. G. *Phys. Rev. B* **2006**, *74*, 214108.
(25) Cao, A. J.; Wei, Y. G.; Mao, S. X. *Appl. Phys. Lett.* **2007**, *90*, 151909.
(26) Jin, Z.-H.; et al. *Scr. Mater.* **2006**, *54*, 1163.
(27) Chen, Z.; Jin, Z.; Gao, H. *Phys. Rev. B* **2007**, *75*, 212104.
(28) Zhu, T.; Li, J.; Samanta, A.; Kim, H. G.; Suresh, S. *Proc. Natl. Acad. Sci. U.S.A.* **2008**, *104*, 3031.
(29) Jin, Z.-H.; et al. *Acta. Mater.* **2008**, *56*, 1126.
(30) Plimpton, S. J. *J. Comp. Phys.* **1995**, *117*, 1. http://lammps.sandia.gov.
(31) Grochola, G.; Russo, S. P.; Snook, I. K. *J. Chem. Phys.* **2005**, *123*, 204719.
(32) Diao, J.; Gall, K.; Dunn, M. L. *J. Mech. Phys. Solids* **2004**, *52*, 1935.
(33) Ackland, G. J.; Jones, A. P. *Phys. Rev. B* **2006**, *73*, 054104.
(34) (a) Shimizu, F.; Ogata, S.; Li, J. *Mater. Trans.* **2007**, *48*, 2923. (b) Li, J. *Modell. Simul. Mater. Sci. Eng.* **2003**, *11*, 173.
(35) Zhang, Y.; Huang, H. *Nanoscale Res Lett.* **2009**, *4*, 34.

NL803553B